LAWRENCE
LIVERMORE
NATIONAL
LABORATORY

LLNL-TR-412938

Implementation of strength and burn models for plastic-bonded explosives and propellants

J. E. Reaugh

May 12, 2009

Disclaimer

This work performed under the auspices of the U.S. Department of Energy by Lawrence Livermore National Laboratory under Contract DE-AC52-07NA27344.

Implementation of strength and burn models for plastic-bonded explosives and propellants

John E. Reaugh

1. Introduction

We have implemented the burn model described in [1] in LS-DYNA. At present, the damage (porosity and specific surface area) is specified as initial conditions. However, history variables that are used by the strength model are reserved as placeholders for the next major revision, which will be a completely interactive model. We have implemented an improved strength model for explosives based on a model for concrete described in [2]. The model exhibits peak strength and subsequent strain softening in uniaxial compression. The peak strength increases with increasing strain rate and/or reduced ambient temperature. Under triaxial compression, the strength continues to increase (or at least not decrease) with increasing strain. This behaviour is common to both concrete and polymer-bonded explosives (PBX) because the microstructure of these composites is similar. Both have aggregate material with a broad particle size distribution, although the length scale for concrete aggregate is two orders of magnitude larger than for PBX. The (cement or polymer) binder adheres to the aggregate, and is both pressure and rate sensitive. There is a larger binder content in concrete, compared to the explosive, and the aggregates have different hardness. As a result we expect the parameter values to differ, but the functional forms to be applicable to both. The models have been fit to data from tests on an AWE explosive that is HMX based.

The decision to implement the models in LS-DYNA was based on three factors: LS-DYNA is used routinely by the AWE engineering analysis group and has a broad base of experienced users; models implemented in LS-DYNA can be transferred easily to LLNL's ALE 3D using a material model wrapper developed by Rich Becker; and LS-DYNA could accommodate the model requirements for a significant number of additional history variables without the significant time delay associated with code modification.

2. Implementation of non-interactive burn model in LS-DYNA

The non-interactive burn model described in [1] has been implemented in LS-DYNA as a user material 'umat45'. Although it would be preferred to implement the model as a user-supplied equation of state, it was not expedient to do so. The next major revision of the model will interact with the geomechanics-based strength model described in Section 3. The LS-DYNA version being used at AWE (ls971_R2_45644) does not permit the simultaneous application of a user-supplied material and a user-supplied equation of state. A recent communication (May 5, 2009) from Livermore Software Technology Company provided the link to a version that does permit both user materials and equations of state, but we have not tested it yet.

To calculate the time for a flame to propagate from an ignition site requires that information is available for both the global coordinates of the ignition site and of the element being calculated. The index to the nodes comprising an element are passed by

the calling subroutine `urmathn`, which passes the element type as the character set 'solid' for both 2D axisymmetric and 3D simulations. However, different indices are used for 2D and 3D. As a result we have included a flag in the input parameter array 'cm' so that the calling routine can pass the correct index for the nodes belonging to the element being calculated.

On the first ever call to 'umat45,' mnemonic pointers to the material property array, the equation of state property array, and the history array are set, the input parameters are loaded into mnemonic variable names in common blocks, and starting values for history variables are calculated according to the input parameters of initial pressure, temperature, and porosity. The porosity is used to set the initial mass fraction of gas products at the initial temperature and pressure. The first time an element is called, its history variables are initialized. If it is a designated ignition element, the coordinates of that element are saved. Once all ignition elements have been processed, the burn propagation time to each element is calculated (which may require two computational cycles). The pressure-dependent mass-burning rate of the element is multiplied by a fraction that rises linearly from 0, at the time the first node of the element is reached by the flame, to 1 at the time the last node is reached. The intent of this complication is to achieve a smoother mass-burning rate as individual elements become involved in the burning. In the present version, the times are calculated once. Although the flame speed is subsonic, the arrival time at the front is not then subsequently adjusted for element compression or expansion. The use of a level set would clearly be preferable. This would also permit burning around obstacles with the appropriate delay. However, the algorithm for a level-set calculation is not available in LS-DYNA, and we have not added the algorithm ourselves.

During the general computational cycle, the artificial viscosity and energy equations are solved in the user material, using the functional forms for viscosity given by Wilkins [3-5]. The functional form is shown in the text following Table 3. We have not implemented the calculation of the change of distance across a zone in the direction of shock propagation that is discussed in [5]. It is likely that the artificial viscosity is also calculated in LS-DYNA for user materials. If so, we have not determined what coefficients are used, and where the element values of the viscosity are accessible. This additional artificial viscosity will not lead to significant errors by itself. However, there will be an additional contribution to the internal energy density of elements that we are missing. In most of our test cases so far, the pressure rises have been slow. Significant shocks have not developed, so the viscosity is a small perturbation. The artificial viscosity issue will be resolved in a subsequent version so that application to Deflagration-to-Detonation Transition (DDT), where shocks do develop, is more accurate.

As described in [1] the first step for the burn model is to solve for pressure and energy density assuming the previous mass fraction of gas has not changed. If the mass fraction changes (from burning), then the second step recalculates pressure and energy density. Finally, the history variables are updated. The history variables appear in Table 1. The symbols are consistent with the notation in [1]. The next version of the burn model will incorporate the four additional variables used by the strength model described in Section 3.

Table 1. History variables used in the non-interactive burn model

Var#	Symbol	Description
1	S/V	Reserved for specific surface area (surface to volume ratio) [Not used]
2	Ignit	Reserved for ignition parameter [Not used]
3	φ	Porosity
4	$\dot{\varepsilon}$	Reserved for local plastic strain rate [Not used]
5	Ie2	Reserved for integral of the square of the plastic strain rate [Not used]
6	$\dot{\varepsilon}_{ave}$	Reserved for average plastic strain rate [Not used]
7	λ	Mass fraction burned
8	P	Element pressure
9	P_g	Gas pressure
10	P_s	Solid pressure
11	P_m	Matrix pressure
12	P_c	Cold pressure (irreversible part of matrix pressure)
13	e	Element specific energy density (per unit mass)
14	e_g	Gas specific energy density
15	e_s	Solid specific energy density
16	e_m	Matrix specific energy density
17	T_g	Gas temperature (K)
18	T_s	Solid temperature
19	v	Element specific volume (per unit mass)
20	v_g	Gas specific volume
21	v_s	Solid specific volume
22	v_m	Matrix specific volume
23	wlim	Limiting value for recompression of expanded matrix
24	t_{ig}	Ignition time of an element
25	dt_{ig}	Time for ignition to propagate through an element
26	qh	Artificial viscosity for the element
27	Area	Element area (2D) or Volume (3D)

2.1 Input instructions for the burn model using LS-DYNA version ls971_d_R2_45644_jer_4.3

Three input cards are used to specify parameters of the user material. The recommended values are given here in gram-cm-microsecond units in Table 2.

Table 2. Input parameters for non-interactive burn model

MID	ROI	MT	LCM	NHV	IORTHO	IBULK	ISHR
mid	rhoi	45	3	29	0	2	3
IVECT	IFAIL	ITHERM	IHYPER	IEOS			
0	0	0	0	0			
IF3D	BULK	SHEAR					
0. or 1.	0.18	0.02					

MID Material identification
ROI Initial density given by $\rho_0(1-\varphi)$ where $\rho_0 = 1.842$, and φ is the initial porosity
MT User material number 45 for burn model
LCM number of input variables to read in the LS-DYNA input file
NHV number of history variables saved (only 27 are used at present)
IORTHO flag for orthotropic materials
IBULK index in the input variable array that points to the bulk modulus
ISHR index in the input variable array that points to the shear modulus
IVECT flag for scalar (0) or vector (1) implementation
IFAIL failure flag (Not used. Presence of gas keeps the pressure positive)
ITHERM flag for temperature calculation
IHYPER flag for deformation gradient
IEOS equation of state flag
IF3D flag: 0. for 2D, 1. for 3D
BULK bulk modulus
SHEAR shear modulus

There are two additional input files required and expected to be read in the same directory as the LS-DYNA input. The first, '*eos.txt*' is the tabular equation of state for the gas products created with Cheetah 5. Its form is four columns with specific energy density (in units of cal/g), pressure (atmospheres), mass density (g/cm^3), and temperature (K). The table is arranged by isotherms, starting at 270 K. The density increases from lowest to highest. Following the recommendations in [1] the tables have been enlarged over the previous version. The new tables range in density from 10^{-4} to 3.5 g/cm^3. The temperature range is from 270 K to 40,000 K. The 270 K isotherm is above the triple point, so the isotherm does not require the rectification discussed in [1]. The second additional input file, '*burn.param*' includes the parameters needed for the burn model and conversion factors for the gas product Eos table. The parameters are shown here in the same format as the LS-DYNA input in Table 2. However, there is at present no provision to read or ignore character strings from the input file, and no requirement that the data appear in formatted columns or even that there are the same number of columns in a given line. The data is read with the FORTRAN statement:
`read(nn,*,end=sss) (eosp(i),i=1,50).`

Table 3. Input parameters in gm-cm-μs units for the burn model supplemental input file '*burn.param*'

NRHO	NTMP	ECON	PCON	RCON	AS	BS	R1S
56.	15.	4.184e-5	1.01325e-6	1.0	69.69	0.	7.8
R2S	WS	CVS	BULKM	BETAM	VMX	GAM0	RVXC
3.9	0.01	2.e-5	0.36	0.001	1.65	0.5	1.65
FRACQ	CQ	CL	T0	P0	POROS	RHO0	DIA
0.75	4.	0.8	298.	1.e-6	0.05	1.842	0.05
VELF0	POWF	POWP	VELIG	NJIG	JIG1	JIG2	…
0.01	0.666667	1.	0.03	n	iel1	iel2	

JIGN	IDBUG						
ieln	ieldb						

NRHO Number of density entries in the gas equation of state table
NTMP Number of isotherms in the gas equation of state table
ECON Conversion factor. Multiply cal/g to get desired energy density unit
PCON Conversion factor. Multiply atmospheres to get desired pressure unit
RCON Conversion factor. Multiply g/cm^3 to get desired density unit
AS *A*, parameter in the JWL form solid equation of state of the reactant
BS *B*, parameter in the JWL form. This parameter is calculated to make the pressure and temperature of the solid equal to the desired values P0 and T0.
R1S *R*, parameter in the JWL form for the solid
R2S *S*, parameter in the JWL form for the solid
WS ω, Gruneisen-like parameter (γ-1) in the JWL form for the solid
CVS c_v, Specific heat of the solid per unit mass
BULKM *K*, bulk modulus of the solid as used to calculate the matrix pressure
BETAM β, parameter for the matrix pressure
VMX initial relative volume for which the matrix pressure can be positive
GAM0 Γ, Gruneisen parameter for the matrix
RVXC maximum relative volume for which the matrix pressure can be positive
FRACQ fraction of the artificial viscosity allotted to the matrix
CQ C_q, coefficient for the quadratic artificial viscosity
CL C_l, coefficient for the linear artificial viscosity

$$qh = 0, \frac{\dot{v}}{v} \geq 0$$

$$qh = C_q l^2 / v \left(\frac{\dot{v}}{v} \right)^2 - C_l l \sqrt{Pv} / v \frac{\dot{v}}{v}, \frac{\dot{v}}{v} < 0$$

$$l = \sqrt{Area}, 2D$$

$$l = \sqrt[3]{Volume}, 3D$$

where v is the specific volume and P is the pressure of the element.

T0 Initial temperature
P0 Initial pressure
POROS φ, initial porosity (gas-filled volume/total volume)
RHO0 ρ_0, reference density of the solid

DIA d, equivalent sphere diameter for the desired surface to volume ratio

$$\frac{S}{V} = \frac{6}{d}$$

VELF0 v_0, laminar flame speed for unit pressure
POWF pf, power for mass fraction dependence of laminar flame speed, v_l
POWP pp, power for pressure dependence of laminar flame speed

$$v_l = v_0 (1 - \lambda)^{pf} p^{pp}$$

VELIG Velocity of flame propagation through the porous solid. This should be (considerably) less than the sound speed in the hot gas, which is about 0.1 cm/μs
NJIG number of elements assumed to be ignited at time zero (no more than 29 at present)
JIG1 element number of the first ignited element
JIGN element number of the NJIGth ignited element
IDBUG element number desired for debug print statements that include each iteration in the approach to pressure equilibrium each cycle

In addition, four history files are calculated as global sums or averages over all of the energetic material and left in the local directory. The files each comprise two columns of numbers – time and the variable. They can be plotted directly (using, for example, 'gnuplot') or imported into a spread sheet. The file '*mtot*' is the total mass of energetic material (including the factor 2π for 2D axi-symmetric calculations). In these Lagrange calculations, the mass should be constant. The value drifts in our calculations. There is an apparent inconsistency between the calculated element volume in LS-DYNA and our integration of the element specific volume from the strain increments. We calculate the new specific volume by

$$\frac{\Delta v}{v} = \Delta\varepsilon_{xx} + \Delta\varepsilon_{yy} + \Delta\varepsilon_{zz} = \Delta$$

$$v_{new} = v_{old}\frac{1+\Delta/2}{1-\Delta/2}$$

The file '*mburn*' is the mass of energetic material burned. The file '*ffave*' is the mass fraction of energetic material burned. The file '*ppave*' is the mass-weighted average pressure in the energetic material. No provision is made to extend the files upon restart. If the user performs a restart in the same directory, the files are over-written.

We used the test calculations illustrated in [1] to check our implementation in 2D. The results are the same. The new equation of state table affects the results very little. In 3D we have checked that the results are reasonable, where they can be simply checked.

3. Implementation of a geomechanics model in LS-DYNA

The geomechanics model described in [2] has been implemented in LS-DYNA as a user material 'umat44'. The first time the model is called, mnemonic pointers to the material parameter vector 'cm' are initialized and put in a common block for future use. The subroutine is given the stress tensor (as a six-member array) from the previous cycle, but corrected for rigid body rotation in the present cycle, and the strain increment tensor as a six-member array. The new specific volume is calculated as above, and used to calculate the new pressure

$$p_{new} = K\left(\frac{1}{\rho_0 v_{new}} - 1\right)$$

where K is the bulk modulus and ρ_0 the reference density. By not calculating the new pressure incrementally, the volumetric hysteresis caused by tensile failure (described below) can be captured. The stress-deviators are updated elastically, and the equivalent stress of the elastic update calculated. The geomechanics model is called to evaluate the

yield stress with the minimum value of the strain rate, which is taken to be the product of 0.01, *TOL*, and *EPSD0*. The input parameter *TOL* is nominally 10^{-5}, and *EPSD0* is the input strain-rate parameter. If the yield stress exceeds the elastically updated equivalent stress, then the state is elastic and no further work need be done. If not, an iteration is performed to converge on the yield stress.

The figure of merit for the iteration is

$$f = 3G\dot{\varepsilon}_p \Delta t + Y - \tilde{\sigma}$$

where G is the shear modulus, $\dot{\varepsilon}_p$ is the plastic strain rate used to calculate the yield stress Y, Δt is the time step, and $\tilde{\sigma}$ is the equivalent stress calculated by the elastic update. If the absolute value of f is less than *TOL* times the characteristic strength (another input parameter, Y_c) the iteration is deemed to have converged. The maximum plastic strain rate is given by

$$\dot{\varepsilon}_{\max} = \frac{\tilde{\sigma}}{3G\Delta t},$$

and the parameter f is evaluated for that rate. The iteration first halves the interval between $\dot{\varepsilon}_{\min}$ and $\dot{\varepsilon}_{\max}$, replacing the limit by the new value of the strain rate: the lower bound is replaced for for $f < 0$, the upper bound replaced for $f > 0$. Once the interval is less than a 1% of $\dot{\varepsilon}_{\max}$ the method switches to a Newton iteration, with the slope taken as

$$\frac{df}{d\dot{\varepsilon}} = \left(f_{\max} - f_{\min}\right)/\left(\dot{\varepsilon}_{\max} - \dot{\varepsilon}_{\min}\right)$$

$$\dot{\varepsilon}_{new} = \dot{\varepsilon}_{\max} - f_{\max} / \frac{df}{d\dot{\varepsilon}}, \left|f_{\max}\right| < \left|f_{\min}\right|,$$

$$\dot{\varepsilon}_{\min} - f_{\min} / \frac{df}{d\dot{\varepsilon}}, \left|f_{\min}\right| \le \left|f_{\max}\right|$$

where f_{max} is the value of f at $\dot{\varepsilon}_{\max}$. By construction, the new trial strain rate is inside the interval. The use of a Newton solver throughout based on the average slope over the interval $\dot{\varepsilon}_{\min}$ to $\dot{\varepsilon}_{\max}$ results in a slow convergence from above. The use of a Newton solver based on the local slope converges well if the functions are smooth. For our present treatment of the behaviour in tension (see below) the yield surface has discontinuous derivatives.

The calculation of the pressure and strain-rate dependent strength proceeds as follows. First the parameter Ω, which is a measure of damage, is calculated.

$$\Omega = \frac{D\langle \varphi_{old} - \varphi_{cr} \rangle}{1 + D\langle \varphi_{old} - \varphi_{cr} \rangle}$$

where φ_{old} is the previous value of the porosity, D and φ_{cr} are parameters, and the McAuley bracket function $\langle\ \rangle$ [2] takes the value of its argument but with a floor of 0. Then

$$s = s_0 \exp(-\beta\Omega/9)$$

$$m = m_0 \exp(-\beta\Omega/28)$$

$$\delta = \frac{\varepsilon_{pold} + \dot{\varepsilon}_p \Delta t}{\varepsilon_{pold} + \dot{\varepsilon}_p \Delta t + \varepsilon_h}$$

$$R = \left(1 + \frac{\dot{\varepsilon}_p}{\dot{\varepsilon}_0}\right)^{ep}$$

are calculated, where s_0, m_0, β, ε_h, $\dot{\varepsilon}_0$ and ep are parameters, and ε_{pold} is the previous value of the plastic strain. In [2] the value of β is 100, and the value of s_0 is 1 for unbroken material.

A pressure minimum, p_{min}, is calculated

$$p_{\min} = -sRY_cF/m$$

where Y_c is a characteristic strength input parameter, and F is taken to be (1-TOL). We found that using the value 1 occasionally led to a slightly negative (round-off) value of b_1, which does not permit convergence. The parameter b_1 is calculated to be

$$b_1 = s + m\frac{\max(p, p_{\min})}{RY_c},$$

and the equation for x solved by a Newton iteration

$$x^{1/n} + mx/3 = b_1 .$$

The starting value for x is taken to be

$$x_{init} = \min(b_1^n, 3b_1/n),$$

and convergence is achieved when the left and right hand sides of the equation differ by no more than the product of 0.01 and TOL. The strength Y_f is then calculated as

$$Y_f = xRY_c,$$

and the yield stress Y is given by

$$Y = Y_f[\delta + C(1-\delta)]$$

where C is an input parameter.

We found it necessary to provide extra logic for the treatment of this material in tension. This tension regime is often the Achilles heel for strength models that incorporate pressure dependence. For such materials, in accordance with experiment, the strength in tension is much smaller than the strength in compression. A factor of 10 is not uncommon for rocks, and nearly that for concrete. The finite difference equations of hydrodynamics, when applied to elastic materials, exhibit dispersion, so that the short wavelength signals propagate too slowly. This is exacerbated when the time step used is significantly smaller than would be permitted by the elastic mesh. The fluctuations that result from shedding the high-frequency components can be of order 10% of the main signal. Linear viscosity [5] improves, but does not eliminate the problem. The end result is that fracture in these materials is often the response to numerical noise.

A second source of unphysical tension can be caused by boundary conditions. The shotgun (frangibility) test [6] is a common standardized test used to establish the mechanical robustness (or its lack) of propellants and explosives. Here a right-circular cylinder (L/D ~ 1.5) impacts an unyielding flat plate with a velocity in the range of 50 to 250 m/s. The propellant or explosive shatters, and the pieces collected and burned in a

pressure vessel [6]. The measured pressure history can be used to calculate the effective surface area of the fragments. Computer simulations of the Taylor test [7] often use the artifice of an unmoving boundary for the impact interface. For metals, where the strength in tension and compression is the same, the artificial tensile stress at the interface, when the cylinder tries to rebound briefly from the impact plate, causes no difficulty. The resulting final length is the same, whether void opening at the interface is permitted or not. When a pressure-dependent strength is used, however, there is a significant difference in the results when void opening is or is not permitted.

The simple answer for Lagrange codes is, of course, to permit void opening. The answer for Eulerian and ALE calculations where the boundary between two materials is a mixed cell, is not simple at all. Indeed, unless an interface orientation is kept, the correct treatment may not be possible. We have incorporated two additional parameters to treat the behavior in tension. The first is the minimum strength, Y_{min}. This can be used to represent an effective strength/adhesion of the binder, which is one of the significant differences between propellants and explosives, on the one hand, and geologic materials and concrete, on the other. The parameter Y_{min} is used by

$$Y = \max\left\{Y_f\left[\delta + C(1-\delta)\right], Y_{\min}\right\}$$

The second input parameter is the fracture strength, P_{frac}. If the pressure is less than P_{frac} in unfractured material, then the fracture flag is set and all stresses are set to zero. If the element is recompressed, the pressure can be compressive. Once the fracture flag is set, the subsequent fracture stress is zero. To permit this hysteresis, the pressure must be calculated as a function of volume, not incrementally.

If, as a result of the combination of mesh resolution and the computer simulation program's treatment of mixed elements there is an unphysically large number of failed elements, the user may wish to incorporate correspondingly unphysical minimum strength and tensile failure strength. Our recommended values for these two parameters are tentative at best. The algorithm only checks for tensile failure after it has calculated a converged strength. In that way a more physically based normal stress criterion can be added in the future.

The porosity is then updated by the following equations

$$\frac{dY}{dp} = \frac{m[\delta + C(1-\delta)]}{\frac{1}{n}x^{(1/n)-1} + m/3}, \quad Y > Y_{\min}$$

$$0, \quad Y = Y_{\min}$$

$$A = \frac{A_0 + A_1 \dfrac{dY}{dp}}{1 + \dfrac{dY}{dp}}$$

$$\frac{d\varphi}{dt} = A\frac{dY}{dp}\dot{\varepsilon}_p(1-\varphi)\,.$$

$$\varphi = \varphi_{old} + \frac{d\varphi}{dt}\Delta t$$

Note that we do not include the expanded volume that results from fracture in the calculation of porosity. Our picture is that the porosity used for strain softening is sub-element size, and distributed uniformly throughout the element. In contrast the extra volume that opens in fracture is element-sized and localized near a fracture plane.

The history variables available for plotting are given in Table 4 below. At present the surface to volume ratio and the ignition parameter are calculated as described in [8]. The equations repeated below. The average plastic strain rate [9] has the property that it is unaffected by long periods of time when no strain is being imposed. It is given by

$$\dot{\varepsilon}_{ave} = \frac{\int_0^t \dot{\varepsilon}^2 dt}{\int_0^t \dot{\varepsilon} dt}$$

Table 4. History variables for geomechanics model

Var#	Symbol	Description
1	S/V	Surface to volume ratio
2	Ignit	Ignition parameter
3	φ	Porosity
4	$\dot{\varepsilon}$	Local plastic strain rate
5	Ie2	Integral of the square of the plastic strain rate
6	$\dot{\varepsilon}_{ave}$	Average plastic strain rate
7	μ	Excess compression = v_0/v - 1
8	frac	Flag set when p < P_{min}
9	minp	Minimum pressure experienced by an element
10	wplas	Plastic work done on the element

The minimum pressure can be examined in post-processing to establish requirements for the input parameter P_{frac} in subsequent calculations. The plastic work is calculated and saved as a potential alternative dependent variable to plastic strain for calculating the specific surface area.

The model as presently formulated ignores the effect of internal energy density (through temperature) on strength. If it were desired to calculate the effect of internal heating from mechanical work on the strength, then the SHPB data would require minor recalibration. Since the SHPB pulse length is about 100 μsec, only the outermost 3 μm of the sample can be cooler than the temperature rise for adiabatic deformation. At 2000 sec^{-1}, the adiabatic temperature rise in the SHPB sample is about 1 K, which corresponds to a 3% reduction in strength. With higher confinement, such as occurs in Steven and spigot tests, the correction will be somewhat larger.

3.1 Input instructions for the geomechanics model using LS-DYNA version ls971_d_R2_45644_jer_3.5

Six input cards are required to specify the parameters of the geomechanics model. The recommended values are given in Table 5 in gram-cm-microsecond units.

Table 5. Input parameters for the geomechanics model

MID	RO	MT	LCM	NHV	IORTHO	IBULK	ISHR
mid	1.842	44	31	11	0	1	2
IVECT	IFAIL	ITHERM	IHYPER	IEOS			
0	0	0	0	0			
BULK	SHEAR	EPS0	EPSPOW	EPSA	SNORM	NORMP	SHRPOW
0.18	0.02	0.2	1.	80.	0.0005	0.5	5.0
TINIT	TSHIFT	PHICR	D	BETA	YC	S0	M0
293.	0.079910	5.2e-6	134.3	49.7	4.17e-4	7.45	16.8
N	EPSH	EDOT0	EDPOW	C	a	b	A0
0.199	0.082	5.6e-6	0.14	0.015	0.1	0.5	0.
A1	PFRAC	YMIN	FAIL	MAXIT	TOL	IDBUG	
0.99	-0.05	1.e-4	0	40.	1.e-5	0.	

MID Material identification
RO Reference density
MT User material number 44
LCM number if input variables to read in the input file
NHV number of history variables saved (only 10 are used at present)
IORTHO flag for orthotropic materials
IBULK index in the input variable array that points to the bulk modulus
ISHR index in the input variable array that points to the shear modulus
IVECT flag for scalar (0) or vector (1) implementation
IFAIL failure flag (not used – see FAIL below)
ITHERM flag for temperature calculation
IHYPER flag for deformation gradient
IEOS equation of state flag
BULK bulk modulus
SHEAR shear modulus
EPS0 ε_0 used in specific surface area calculation
EPSPOW *pe* used in specific surface area calculation
EPSA *AA* used in specific surface area calculation

$$S/V = AA\left(\varepsilon - \varepsilon_0\right)^{pe}$$

SNORM σ_n, Normal stress used in ignition parameter
NORMP *pn*, power used in normal stress factor of ignition parameter
SHEARP *ps*, power used in shear factor of ignition parameter

$$Ignit = \int \left(\frac{p - s_2/2}{\sigma_n}\right)^{pn} \left(2 - \frac{3|s_2|}{Y}\right)^{ps} d\dot{\varepsilon}$$

, where p is pressure, s_2 is the intermediate principal stress, and Y is the yield stress.
TINIT Ambient temperature, used for shift in the strain-rate dependence
TSHIFT fraction of a decade shift per degree Kelvin different from ambient (293)
PHICR φ_c, used in the calculation of Ω

D D used in the calculation of Ω

BETA β used in the calculation of strength reduction with damage

YC y_c, unconfined compressive strength parameter

S0 s_0 used in pressure-dependent strength calculation

M0 m_0 used in pressure-dependent strength calculation

N n used in pressure-dependent strength calculation

EPSH e_h used in strain-hardening term (δ)

EDOT0 $\dot{\varepsilon}_0$ used in strain-rate dependent term

EDOTP ep used in strain-rate dependent term

C C used in damage softening

a a used in calculation of unloaded porosity from porosity under stress [not used in the present version]

b b used in calculation of unloaded porosity [not used in the present version]

A0 A_0 used in calculation of porosity increase with strain rate (bulking rate)

A1 A_1 used in calculation of porosity increase with strain rate

PFRAC Fracture parameter

YMIN Minimum strength

FAIL used to set failed element flag if element reaches P_{frac} criterion. FAIL less than one does not set the flag, FAIL greater than or equal to one does set the flag. In LS-DYNA failed elements are removed from the calculation and are blanked for graphics output

MAXIT maximum number of iterations permitted to solve for consistent plastic strain rate. If the criterion is exceeded, the calculation prints a message on the file *'stdout'* and stops.

TOL The criterion for a successful iteration for consistent plastic strain rate is that

$$\left|3G\dot{\varepsilon}\Delta t + Y(\dot{\varepsilon}, \varepsilon, p) - \tilde{\sigma}\right| < (TOL)Y_c$$

This parameter is also used to avoid round off when calculating the pressure dependent strength and elsewhere.

IDBUG additional print statements are added to the file *'stdout'* when the local element number takes on the value *IDBUG*. (not recommended in general)

The recommended values are given in SI units in Table 6 below.

Table 6. Input parameters for the geomechanics model

MID	RO	MT	LCM	NHV	IORTHO	IBULK	ISHR
mid	1.842e3	44	31	11	0	1	2
IVECT	IFAIL	ITHERM	IHYPER	IEOS			
0	0	0	0	0			
BULK	SHEAR	EPS0	EPSPOW	EPSA	SNORM	NORMP	SHRPOW
0.18e11	0.02e11	0.2	1.	80.e2	5.e7	0.5	5.0
TINIT	TSHIFT	PHICR	D	BETA	YC	S0	M0
293.	0.079910	5.2e-6	134.3	49.7	4.17e7	7.45	16.8
N	EPSH	EDOT0	EDPOW	C	a	b	A0
0.199	0.082	5.6	0.14	0.015	0.1	0.5	0.

A1	PFRAC	YMIN	FAIL	MAXIT	TOL	IDBUG	
0.99	-0.05e11	1.e7	0	40.	1.e-5	0.	

3.2 Comparison with experiment

The first parameter set we developed was a result of fitting Split Hopkinson Pressure Bar (SHPB) and modest rate uniaxial compression tests [10] and also quasi-static triax tests [11]. The method used was to select parameter ranges for each of the input parameters, and then select parameters randomly within those ranges, retaining the parameters with the best overall (least squares) fit. This is not a totally satisfactory method.

The use of low temperature to create data at high effective strain rate is not completely satisfactory, and the test results in [10] are only good to an effective strain rate of 3000 sec^{-1}, using their figure of 13.1 K per decade. However the Cavendish Lab had performed some additional tests on the explosive at a nominal strain rate of 2000 sec^{-1}, but with temperatures varying from -100 to 60 C. [12] We found that using the data from -25 C to 60, together with the low strain-rate data at reduced temperature from [7] we were able to get a satisfactory fit to the peak stress with the functional form

$$R = \left(1 + \frac{\dot{\varepsilon}_p}{\dot{\varepsilon}_0 \exp[\alpha(T - T_0)]}\right)^{ep}$$

where $\dot{\varepsilon}_0$ takes the value 5.6 sec^{-1}, α takes the value 0.184 and *ep* takes the value 0.14. The correlation of the Cavendish Lab data for peak stress and this functional form is shown in Figure 1. This value of α is equivalent to the *TSHIFT* parameter value of 0.0799 (about 5% larger than before). The parameters in Tables 5 and 6 are a result of this later fit.

It was noted by Simon Chetwynd [13] that the previous parameter set using only the strain rate data from [10] gave somewhat too stiff response in the Steven test, where the calculated strain rate was about 10,000 sec^{-1}. Those parameters were estimated without the data from [12]. For that case, the value of *ep* was 0.45. The resulting fit using data from both [10] and [12] and the experimental results at strain intervals of 1% are shown in Figures 2 and 3.

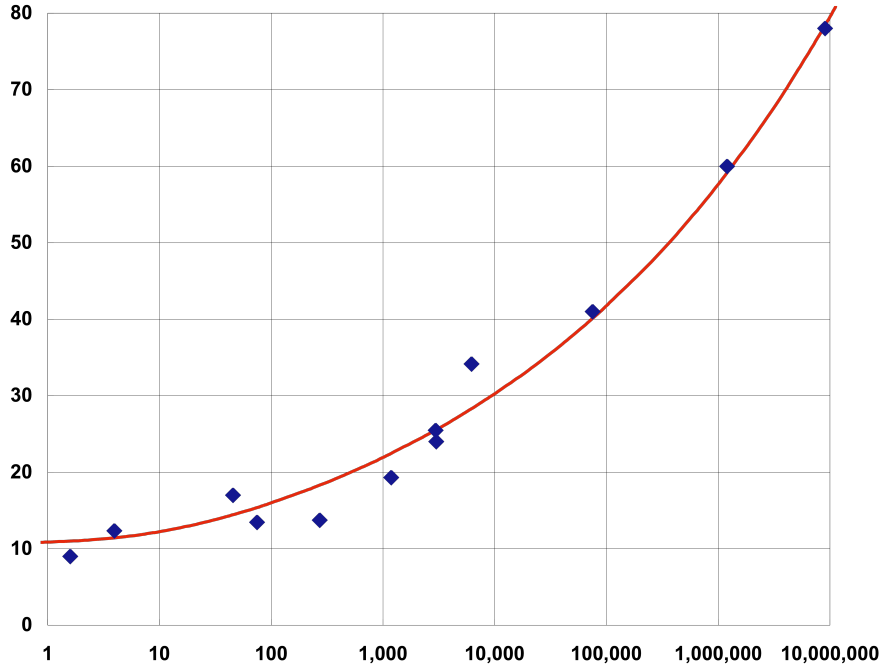

Figure 1. Peak stress, MPa, of SHPB and slow strain-rate testing at various temperatures as a function of strain rate, per second, compared with the model fit (line) described above. The experimental data have been adjusted to be the effective strain rates at room temperature.

We should note that the use of strain softening material models can, in some circumstances, lead to strain localization, and significantly non-uniform deformation. There are some computational and experimental indications that localizations take place in the tests used to establish the strength model. The results for strength are assessed with the assumption that stress and strain are uniform throughout the sample. In cases where the strains are non-uniform, the parameters for a constitutive model can be inferred indirectly by comparing the results of detailed simulations with the measurements. The method was demonstrated by Wilkins and Guinan [7] for the Taylor test, and used in [14] to establish the work hardening of steel during the necking that occurs in a simple tension test.

In Figure 3, the data for 6200 sec^{-1} are actually the results of SHPB tests at reduced temperature, using the temperature strain-rate scaling law fitted above. That test was not used in the fitting process. In Figure 1 the fitted function is seen to lie below the datum at the effective strain rate 6200 sec^{-1}.

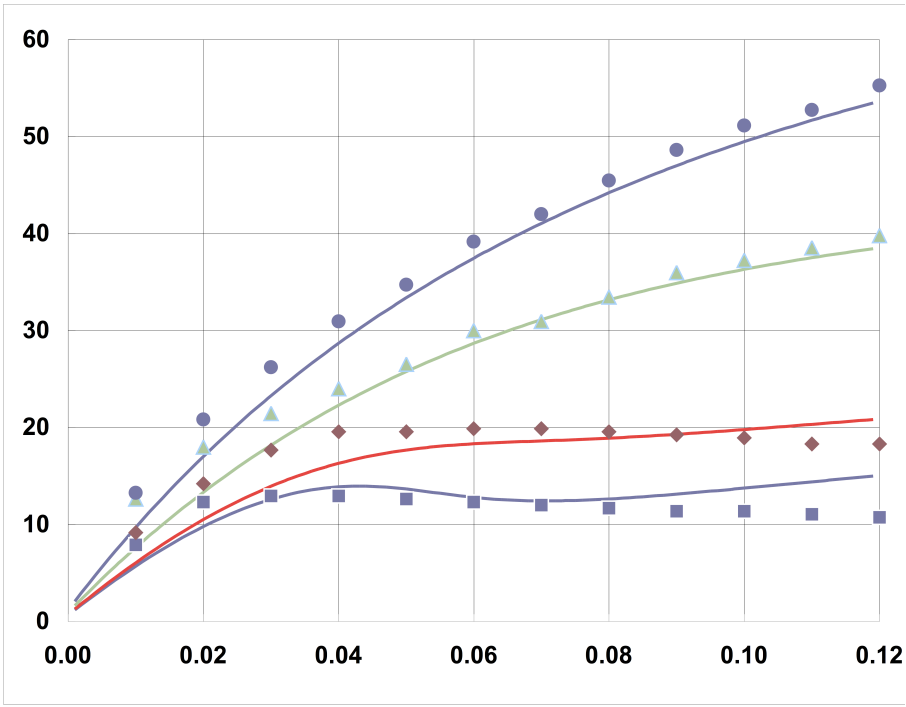

Figure 2. Comparison of model results (lines) with experiments for triax tests at low strain rate. Flow stress, MPa, as a function of strain for lateral stresses of (top to bottom) 140, 35, 7, and 3.5 MPa [11]

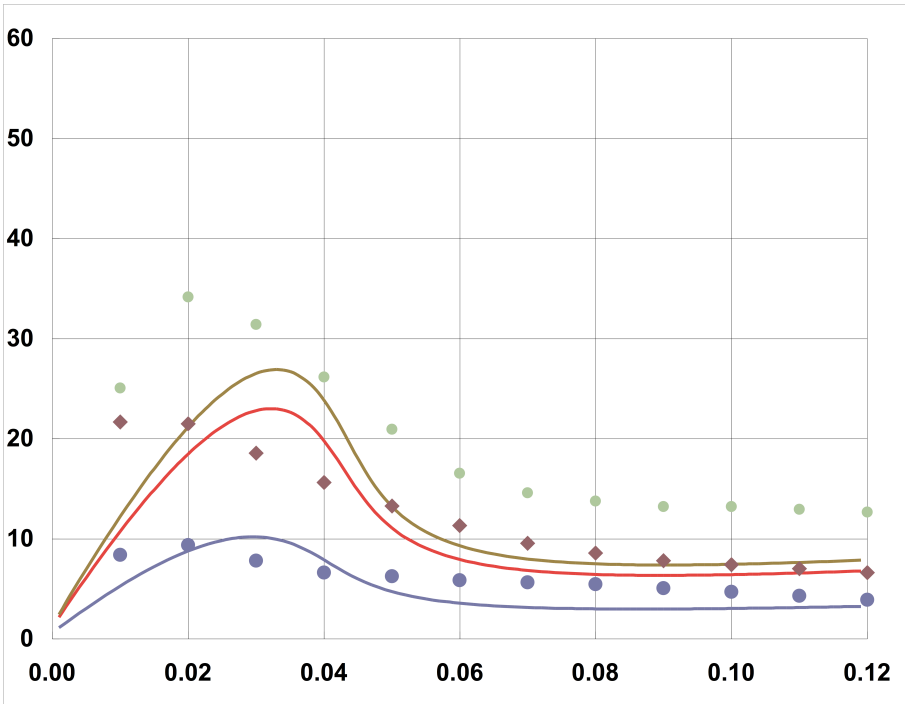

Figure 3. Comparison of model results (lines) with experiments for SHPB tests at various strain rates. Flow stress, MPa, as a function of strain for strain-rates of (top to bottom) 6200 (not used in the fitting process), 2000, and 0.13 sec^{-1}.

4. Summary, plans and schedule

At this point, the two major pieces of the HEVR model have been completed and implemented in the same computer simulation program. The first piece is the multi-species, single velocity approximation to the burning of a porous explosive. This piece of the model can be used to assess the effects of confinement on the amount of explosive burned, and the time taken to burn, using the specific surface area and porosity as free parameters. The second piece is a constitutive model for the explosive that depends on strain-rate and confining pressure, and exhibits both strain hardening and strain softening when the confining pressure is sufficiently low.

The next major revision of the model is planned for implementation in August 2009. This will be an interactive model, so that the explosive is damaged in a test vehicle, and at a time and location determined by the ignition parameter begins to burn. The flame propagates through damaged material and ignites the surface area created there. Pressure builds up in the distorted test vehicle, and is relieved as the confinement fails.

In parallel, AWE has produced the first draft of a validation plan to assess the constitutive model when applied to a number of different test vehicles. The model results will be compared with the test results, and the region of validity determined. A similar validation plan for the burn model will require special testing for deliberate ignitions in explosive with significant specific surface area (either damaged material or possibly moulding powder) at various initial porosities. This testing may include deflagration-to-detonation testing geometry (strong confinement, planar ignition, and planar propagation) and HEVR geometry (modest or weak confinement, point or localized ignition, and diverging propagation.

A report on the interactive model will be prepared and issued in September 2009. That report will include discussion of the model status, and a schedule for a prioritized list of further improvements and refinements.

5. References

1. J.E. Reaugh, “Calculating the Dynamics of High Explosive Violent Response (HEVR) after Ignition, LLNL report LLNL-TR-407915, October 2008.
2. O.Yu. Vorobiev, B.T. Liu, I.N. Lomov, T.H. Antoun, “Simulation of penetration into porous geologic media,” *Int. J. Impact Engineering*, **34**, p721, April 2007.
3. M.L. Wilkins, “Calculation of Elastic-Plastic Flow,” in *Methods in Computational Physics, Vol. 3: Fundamental Methods in Hydrodynamics*, B. Alder, ed., Academic Press, 1964.
4. M.L. Wilkins, *Computer Simulation of Dynamic Phenomena*, Springer, 1999.
5. M.L. Wilkins, “Use of Artificial Viscosity in Multidimensional Fluid Dynamic Calculations,” *J. Computational Physics*, **36**, p281, 1980.
6. A.I. Atwood, K.P. Ford, D.T. Bui, P.O. Curran, T.M. Lyle, “Assessment of mechanically induced damage in solid energetic materials,” *7th Int. Symposium on Special Topics in Chemical Propulsion*, Kyoto, Japan, September, 2007.
7. M.L. Wilkins and M.W. Guinan, “Impact of cylinders on a rigid boundary,” *J. Appl. Phys.*, **44**, p1200, 1973.
8. J.E. Reaugh, “Progress in model development to quantify High Explosive Violent Response (HEVR) to mechanical insult,” LLNL report LLNL-TR-405903, August 2008.

9. J.L. Maienschein, J.E. Reaugh, E.L. Lee, "Propellant Impact Risk Assessment Team Report: PERMS Model to Describe Propellant Energetic Response to Mechanical Stimuli," LLNL report UCRL-ID-130077, February 1998.
10. D.M. Williamson, C.R. Siviour, W.G. Proud, S.J.P. Palmer, R. Govier, K. Ellis, P. Blackwell, and C. Leppard, "Temperature-time response of a polymer bonded explosive in compression," *J. Phys. D: Appl. Phys.* **41**, 085404, 2008.
11. D.A. Wiegand, B. Reddingius, K. Ellis, and C. Leppard, "Mechanical failure properties of a polymer composite as a function of hydrostatic pressure," (to be published), *J. Mechanics and Physics of Solids*, 2009.
12. D.R. Drodge, S.J.P. Palmer, D.M. Williamson, W.G. Proud, and J.E. Field, "2nd Quarterly Report 2007, Mechanical and Microstructural Properties of Polymer Bonded Explosives, April 2007.
13. Simon Chetwynd, AWE, private communication, 2009.
14. J. E. Reaugh, A. C. Holt, M. L. Wilkins, B. J. Cunningham, B. L. Hord, and A. S. Kusubov, "Impact Studies of Five Ceramic Materials and Pyrex," *Int. Journal Impact Engrg.* **23** (1999) 771-782